THE JOURNAL OF PHYSICAL CHEMISTRY A

pubs.acs.org/JPCA

Article

# Vibrational Spectra of the Ruthenium−Tris-Bipyridine Dication and Its Reduced Form in Vacuo

*Published as part of The Journal of Physical Chemistry virtual special issue "International Symposium on Molecular Spectroscopy".*

Musleh Uddin Munshi, Jonathan Martens, Giel Berden, and Jos Oomens*

Cite This: *J. Phys. Chem. A* 2020, 124, 2449−2459

Read Online

ACCESS | Metrics & More | Article Recommendations | Supporting Information

**ABSTRACT:** Experimental IR spectra in the 500−1850 $cm^{-1}$ fingerprint frequency range are presented for the isolated, gaseous redox pair ions $[Ru(bpy)_3]^{2+}$, and $[Ru(bpy)_3]^{+}$, where bpy = 2,2′-bipyridine. Spectra are obtained using the FELIX free-electron laser and a quadrupole ion trap mass spectrometer. The 2+ complex is generated by electrospray ionization and the charge-reduced radical cation is produced by gas-phase one-electron reduction in an ion−ion reaction with the fluoranthene radical anion. Experimental spectra are compared against computed spectra predicted by density functional theory (DFT) using different levels of theory. For the closed-shell $[Ru(bpy)_3]^{2+}$ ion, the match between experimental and computed IR spectra is very good; however, this is not the case for the charge-reduced $[Ru(bpy)_3]^{+}$ ion, which demands additional theoretical investigation. When using the hybrid B3LYP functional, we observe that better agreement with experiment is obtained upon reduction of the Hartree−Fock exact-exchange contribution from 20% to about 14%. Additionally, calculations using the M06 functional appear to be promising in terms of the prediction of IR spectra; however, it is unclear if the correct electronic structure is obtained. The M06 and B3LYP functionals indicate that the added electron in $[Ru(bpy)_3]^{+}$ is delocalized over the three bpy ligands, while the long-range corrected LC-BLYP and the CAM-B3LYP functionals show it to be more localized on a single bpy ligand. Although these latter levels of theory fail to reproduce the experimentally observed IR frequencies, one may argue that the unusually large bandwidths observed in the spectrum are due to the fluxional character of a complex with the added electron not symmetrically distributed over the ligands. The experimental IR spectra presented here can serve as benchmark for further theoretical investigations.

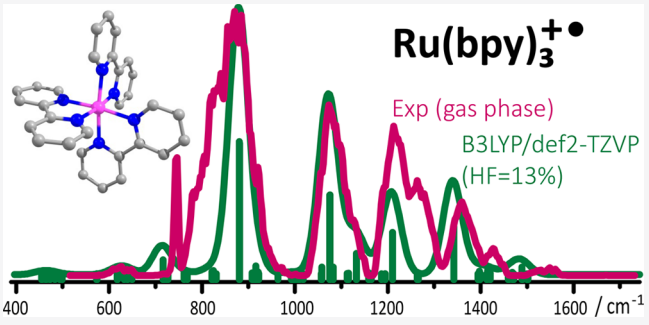


## 1. INTRODUCTION

The tris(2,2′-bipyridine)−ruthenium coordination complex ion $[Ru(bpy)_3]^{2+}$ is a classical metal−organic ingredient used, for instance, in dye-sensitized solar cells (DSSCs),[1−6] in sensors,[7,8] in organic synthesis as a photoredox catalyst,[9−11] and in artificial photosynthetic schemes.[12−14] The dicationic $[Ru(bpy)_3]^{2+}$ coordination complex is known to possess a high absorption cross section in the visible range of the spectrum. In DSSCs, light absorption occurs predominantly on transitions with metal-to-ligand charge-transfer (MLCT) character,[15] leading eventually to oxidation of the dye. The oxidized dye is reduced back typically by the $I^-/I_3^-$ redox shuttle in solution (Figure 1).[16,17] $[Ru(bpy)_3]^{2+}$ may also be reduced to $[Ru(bpy)_3]^{+}$ by accepting an electron before photo-oxidation (reductive quenching).[18] These successive reductions give rise to a series of oxidation states of the dye sensitizer.[14] Structure, stability, excited state reactivity, and photodynamics are dependent on the oxidation state, and studies of these complexes in complete isolation can contribute to a better understanding of their properties. One particularly interesting aspect of gas-phase studies is that they can serve as critical benchmarks for high-level theoretical models used to describe these systems.

In order to unravel the underlying mechanisms at each stage, $Ru(bpy)_3$ and many of its derivatives have been the subject of a vast number of experimental and theoretical studies.[5,6,15,19−26] The long-term stability of the dyes used in DSSCs is a crucial issue in their practical applicability. For instance, although $Ru(bpy)_3$-based complexes exhibit solar-cell efficiencies of about 11% in outdoor conditions,[16,27−29] they degrade over time[30,31] and reductive quenching[16] influences the efficiency.

**Received:** January 31, 2020
**Revised:** March 2, 2020
**Published:** March 2, 2020

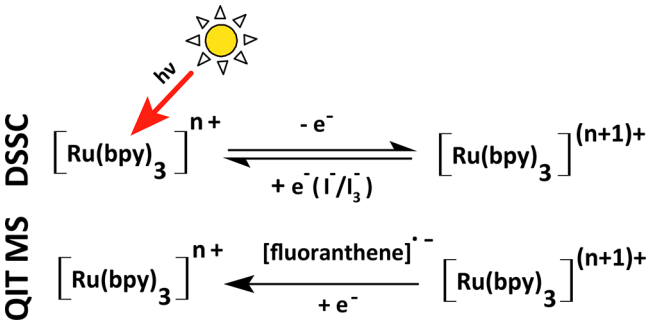


**Figure 1.** Schematic representation of the key redox reactions in the dye-sensitized solar cell (DSSC) and the generation of the redox pairs through charge reduction via one-electron addition in the quadrupole ion trap mass spectrometer (QIT MS).

Various structural fabrications have been suggested, such as replacement of monodentate thiocyanate ligands by anionic aromatic tris(bidentate) or bis(tridentate) ligands.[32−41] The excited state reactivity is another crucial factor in their design. For instance, tris(bidentate) complexes have relatively long excited state lifetimes compared to those of bis(tridentate) complexes.[19,42] Longer lifetimes of the excited states may induce dissociation of the dye sensitizers and degrade their performance over time. In contrast, the fast regeneration of the oxidized species may prevent degradation.

Infrared and resonance Raman spectroscopy were employed to study the $[Ru(bpy)_3]^{2+}$ ion[26,43] and its deuterated analogue in solution along with valence force field[44,45] calculations to assign the observed vibrational bands.[46] Transient infrared absorption spectroscopy[47,48] was used to study the ground and the excited triplet MLCT state of $[Ru(bpy)_3]^{2+}$ in solution.[49,50] It was concluded that the excited electron is localized on one of the bpy ligands rather than being delocalized over all ligands.[43,51] A similar conclusion was also proposed for the reduced $[Ru(bpy)_3]^{+}$ ion in solution on the basis of different types of spectroscopy.[52−54] In contrast, gas-phase electronic spectroscopy experiments on the $[Ru(bpy)_3]^{+}$ ion and associated computations suggested that the added electron is delocalized over the three bpy ligands.[55]

The energy required to remove a bpy ligand from the dication is naturally higher than from the monocation analogue, which was shown experimentally using gas-phase photodissociation in the visible wavelength range.[55,56] In these experiments, gaseous $[Ru(bpy)_3]^{+}$ was prepared by charge reduction of $[Ru(bpy)_3]^{2+}$ by electron transfer from cesium vapor. The UV spectrum of the monocation showed much broader bands than that of the dication analogue, where bands were also red-shifted with respect to those for the dication. Here, we investigate the same gaseous $Ru(bpy)_3$ complex in the 1+ and 2+ oxidation states using IR spectroscopy in the fingerprint range and address the question of whether the change of oxidation state from 2+ to 1+ affects the IR spectrum and structure of the complex.

Numerous electronic structure calculations have been reported for the $[Ru(bpy)_3]^{2+}$ ion.[57−60] Especially density functional theory (DFT) has been extensively used to predict physicochemical properties of the system. For experimental validation of these computational results, gas-phase experiments are especially valuable as solution-phase studies may lack species selectivity and may show unwanted or unknown effects of solvent molecules or counterions, which obstruct a clear understanding of intrinsic molecular properties.[61] However, the availability of gas-phase data on these ionic systems is limited due to experimental challenges. Here, we provide gas-phase IR spectra of isolated $[Ru(bpy)_3]^{2+}$ and its charge-reduced $[Ru(bpy)_3]^{+}$ counterpart. Our methodology is based on IR multiple-photon dissociation (IRMPD) spectroscopy of mass-selected ions in a quadrupole ion trap mass spectrometer (QIT-MS).[62−64] $[Ru(bpy)_3]^{2+}$ ions are produced by electrospray ionization (ESI) and its reduced analogue is produced in a gas-phase electron-transfer reaction with an anionic reagent,[65] thus giving unique spectroscopic access to the two members of the redox-pair in complete isolation.[66] We compare our experimental spectra with DFT computed IR spectra and with relevant data derived from previous gas-phase electronic spectra of bare[55] and tagged[56,67−69] $Ru(bpy)_3$ ions.

## 2. METHODS

**2.1. Experimental Section.** All experiments have been performed in a modified quadrupole ion trap mass spectrometer (QIT MS, Bruker, AmaZon Speed ETD, Bremen, Germany), which has been described in detail elsewhere.[62] The dication of interest, $[Ru(bpy)_3]^{2+}$ was generated via ESI starting from a solution containing a few $\mu$M $[Ru(bpy)_3]Cl_3$ salt and 10 $\mu$M bpy in 1:1 MeOH:$H_2O$. The $[^{102}Ru(bpy)_3]^{2+}$ ion at $m/z$ 285 was mass-isolated, retaining only the 102-isotope of ruthenium. Then, from the isotopically pure dication, the charge-reduced $[^{102}Ru(bpy)_3]^{+}$ ion at $m/z$ 570 is generated by one-electron charge reduction using the electron-transfer dissociation (ETD) option of the QIT-MS.[55,65,66,70] During the charge-reduction reaction, an electron is transferred from the fluoranthene radical anion to the Ru-complex dication. Fluoranthene radical anions are generated in a negative chemical-ionization ion source and are transferred to the quadrupole trap, where they engage in an ion−ion reaction for 250−300 ms with the $[^{102}Ru(bpy)_3]^{2+}$ dication.[66,71] The intact charge-reduced monocation (sometimes referred to as ETnoD) can then be mass-isolated for subsequent IRMPD spectroscopic interrogation.

Fingerprint IRMPD spectra of both $[Ru(bpy)_3]^{2+/+}$ ions were recorded from 500 to 1850 $cm^{-1}$ using the tunable infrared radiation from the FELIX free-electron laser (FEL).[63,64] Operating at a repetition rate of 10 Hz, FELIX[72,73] produces macropulses of 6−10 $\mu$s duration with energies up to 100 mJ per pulse. The mass-to-charge isolated ions are irradiated with the FEL radiation, which induces vibrational excitation when the laser frequency is on-resonance with one of the normal modes of the ions. Multiple photons are absorbed while statistical redistribution of energy takes place, thus increasing the internal energy of the ions, eventually leading to unimolecular dissociation. $[Ru(bpy)_3]^{2+}$ ions were irradiated with 20 FEL macropulses at maximum pulse energy. The charge-reduced ions, $[Ru(bpy)_3]^{+}$, were irradiated by 2 pulses with the pulse energy reduced by a factor of 3 to prevent saturation by complete depletion of the precursor ions. IR spectra were generated by plotting the natural logarithm of the fragmentation yield

$$-\ln\left[1 - \sum I_{frag}/\left(I_{pre} + \sum I_{frag}\right)\right]$$

as a function of the IR laser frequency, where $I_{frag}$ and $I_{pre}$ represent ion intensities for fragment and precursor ions, respectively.[74,75] At each IR frequency point, five mass spectra were averaged. The laser frequency step size was 3 $cm^{-1}$. The yield is linearly corrected for frequency-dependent variations in


https://dx.doi.org/10.1021/acs.jpca.0c00888
J. Phys. Chem. A 2020, 124, 2449−2459

the laser pulse energy and the IR frequencies are calibrated using a grating spectrometer.

**2.2. Computational Modeling.** Geometries were optimized at several levels of theory to test the applicability of various functionals for these particular systems. The B3LYP[76,77] and range-separated[78] LC-BLYP levels of theory were used with the def2-TZVP[79,80] basis set for all atoms. Additionally, B3LYP and several meta functionals developed by the Truhlar group[81] (M06, M06L, M06-2X) were employed for comparison with an effective core pseudopotential (ECP) on Ru and 6-311+G(d,p) on C, N, and H atoms.[82] The range-separated CAM-B3LYP level of theory was also used for the charge-reduced monocation. In all cases, the ECP used was aug-cc-pVTZ-pp.[83] To refine the relative energies among different functionals, single-point MP2/6-311+G(2d,2p) calculations were also performed. Relativistic effects were not taken into account using these functionals. Natural population analysis (NPA)[84] was performed using the keyword "pop = npa". All calculations described above were performed using Gaussian09 revision D 01.[85]

Alternatively, the Amsterdam Density Functional (ADF) program package[86−88] was used. The B3LYP, M06, and O3LYP (developed by Cohen and Handy[89]) functionals were employed with uncontracted Slater type orbitals (STOs) of triple-$\zeta$ quality including two sets of polarization basis functions (TZ2P[90]). The hybrid O3LYP[89] functional is similar to the B3LYP functional but uses 12% HF exact exchange instead of 20% in B3LYP. Relativistic effects were taken into account using the Zero-Order Regular Approximation (ZORA) method[91−94] within the ADF program package.

With the optimized geometries (see Figure 2), vibrational frequencies were calculated within the harmonic approximation. All stationary points were confirmed to be true minima with no imaginary frequencies. Doubly charged Ru(II) has a $d^6$ electron configuration, and a singlet spin configuration was chosen in all calculations. The charge-reduced Ru(I) has a $d^7$-configuration and a doublet spin state was chosen within an approximately octahedral ligand environment (Figure 2).

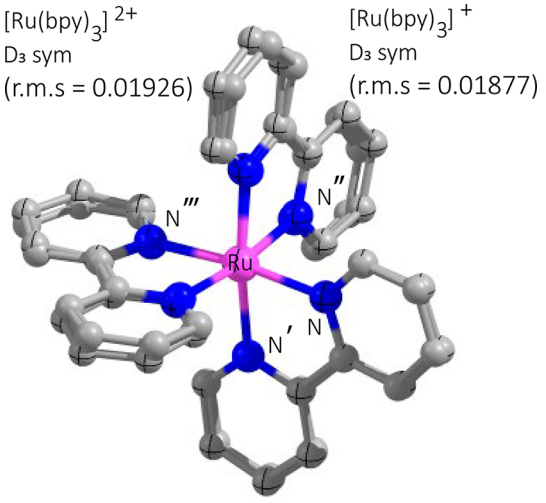


**Figure 2.** DFT computed structure of $[Ru(bpy)_3]^+$ overlaid with that of $[Ru(bpy)_3]^{2+}$ at the M06 level of theory. The structures are similar (Table 2), possessing $D_3$ symmetry, but their fingerprint IR spectra (500−1850 $cm^{-1}$) are significantly different (see Figure 4). Hydrogen atoms are omitted for clarity. Coordinate labeling as used in Table 2 is shown.

Computed harmonic IR frequencies were convoluted using a 15 $cm^{-1}$ full-width at half-maximum (fwhm) Gaussian line shape function. For consistency in evaluating the performance of different levels of theory in terms of IR spectral prediction, we chose to scale harmonic frequencies by a factor of 0.965 for all levels of theory. This scale factor gives satisfactory results for the dicationic species when B3LYP or M06 functionals are used (see Figure 4).

## 3. RESULTS AND DISCUSSION

**3.1. $MS^n$ Results.** The mass spectrum recorded after electrospray ionization of the $[Ru(bpy)_3]Cl_3$ solution is shown in Figure 3a. Clearly visible is the $[Ru(bpy)_3]^{2+}$ ion peak with its characteristic isotope pattern, which is enlarged in the inset, Figure 3b. After the $^{102}$Ru-containing species were isolated at $m/z$ 285, the ions were resonantly irradiated with the FEL at 1436 $cm^{-1}$. The main fragment is found at $m/z$ 157 corresponding to a protonated bpy ligand, with the complementary ion barely visible at $m/z$ 413, corresponding to $[Ru(bpy)(bpy\text{-}H)]^+$; see Figure 3c. An additional fragment is found at $m/z$ 207, which is attributed to the $[^{102}Ru(bpy)_2]^{2+}$ ion, an undercoordinated 2+ ion, that easily picks up a background water molecule in the QIT resulting in a mass peak at $m/z$ 216.

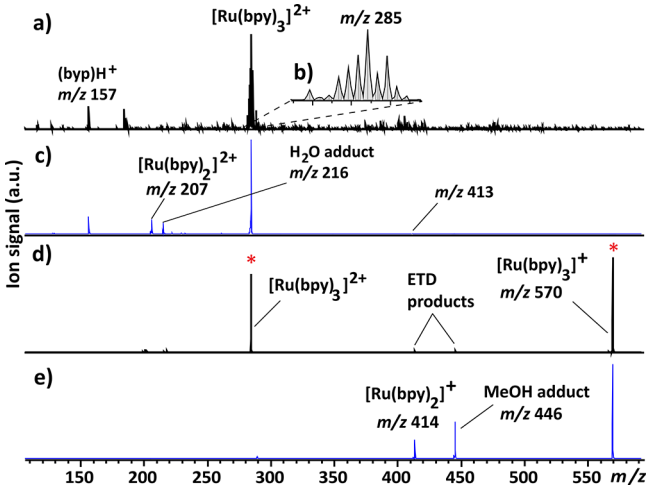


**Figure 3.** Mass spectra of (a) ESI of the Ru-bpy solution generating $[Ru(bpy)_3]^{2+}$ with its main isotopologue at $m/z$ 285. (b) shows an expanded view of the isotope distribution of $[Ru(bpy)_3]^{2+}$. (c) Infrared photodissociation of isolated $[^{102}Ru(bpy)_3]^{2+}$. (d) Electron-transfer reduction of isolated $[^{102}Ru(bpy)_3]^{2+}$ showing a peak corresponding to the formation of the charge-reduced $[^{102}Ru(bpy)_3]^+$ ion at $m/z$ 570, as well as ETD-induced fragments at $m/z$ 414 and $m/z$ 446. (e) Infrared photodissociation of isolated $[^{102}Ru(bpy)_3]^+$.

In a separate experiment, the mass-isolated $[^{102}Ru(bpy)_3]^{2+}$ ion was charge-reduced using the fluoranthene radical anion form the ETD source, resulting in the singly charged $[^{102}Ru(bpy)_3]^+$ ion at $m/z$ 570 (Figure 3d). The ETR reaction time was optimized to maximize the amount of charge-reduced ions. In this particular ETR reaction, approximately 55% of the dication is charge-reduced. After mass isolation, the $[Ru(bpy)_3]^+$ ion was resonantly irradiated by the FEL at 1360 $cm^{-1}$, which primarily produced a fragment at $m/z$ 414, which can be attributed to the $[Ru(bpy)_2]^+$ ion (Figure 3e). Additionally, a peak at $m/z$ 446 is observed, which is presumably a methanol adduct of $[Ru(bpy)_2]^+$.


https://dx.doi.org/10.1021/acs.jpca.0c00888
J. Phys. Chem. A 2020, 124, 2449−2459

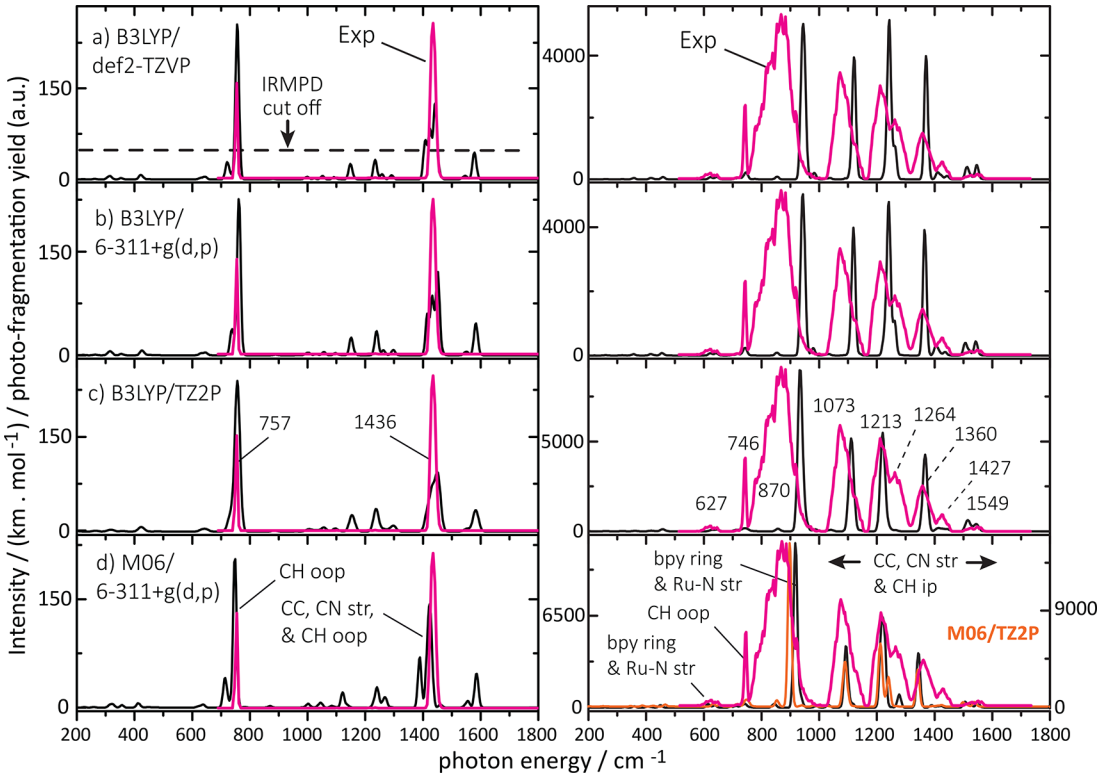


**Figure 4.** Gas-phase experimental IRMPD spectra (magenta) of $[Ru(bpy)_3]^{2+}$ (left) and charge-reduced $[Ru(bpy)_3]^{+}$ (right), overlaid with calculated IR spectra (black) using several levels of DFT. Additionally, the M06/TZ2P predicted spectrum for the monocation is shown in orange in panel d (intensity on the right). Experimental band maxima are labeled (panel c), and their approximate dominant mode characters are also indicated (panel d). Computed spectra for the dication are in good agreement with experiment at all levels of theory at the selected scaling factor of 0.965. Some weak bands are not observed, which we attribute to nonlinearity of the IRMPD process leading to an apparent cutoff (dashed line) for this strongly bound complex. For the monocation, the IR frequencies show significantly more variation. The M06 method appears to outperform others (panel d).

**3.2. Comparison of the IR Spectra of $[Ru(bpy)_3]^{2+}$ and $[Ru(bpy)_3]^{+}$.** The IRMPD spectrum of $[Ru(bpy)_3]^{2+}$ is shown in the left-hand panels of Figure 4 and reveals only two dominant relatively narrow IR absorption bands. Substantial changes in the IRMPD spectrum are observed upon charge reduction to $[Ru(bpy)_3]^{+}$, whose spectrum shows an increased number of strong IR bands, which are also significantly broadened (see right-hand panels in Figure 4 and Table 1). In previous studies on charge-reduced coordination complexes of Ni and Cu performed under similar experimental conditions,[66,95] such obvious spectral broadening was not observed, suggesting that the broadening is intrinsic to the $Ru(bpy)_3^{+}$ system and not to the experimental method. Theoretical IR spectra (black in all panels) at all levels of theory produce a relatively satisfactory match for the dication. However, this is not the case for the charge-reduced monocation, for which the predicted frequencies of the main absorption bands are severely blue-shifted. The M06 functional appears to give the closest match with the experimental frequencies.

The energetic requirements to induce dissociation of the complex are very different for the two oxidation states. To record the IRMPD spectra in Figure 4, the $[Ru(bpy)_3]^{2+}$ ions were irradiated by 20 laser pulses, whereas the charge-reduced $[Ru(bpy)_3]^{+}$ ions were irradiated by only 2 pulses, attenuated to one-third of the original pulse energy. This is in qualitative agreement with observations by Nielsen and co-workers, who investigated these ions by gas-phase UV/vis photodissociation spectroscopy.[55,56] In the literature, experimental gas-phase bond dissociation energies for the loss of a bpy ligand from $M(bpy)_2^{+}$ complexes were reported by Rodgers and co-workers[96−98] to be 2.33 eV for Zn, 2.46 eV for Cu, and 2.81 eV for Ni. We calculate a value of 3.59 eV for the loss of a bpy unit from $[Ru(bpy)_2]^{+}$ and 6.55 eV from $[Ru(bpy)_2]^{2+}$. For the complex with three ligands, Nielsen and co-workers calculated (B3LYP/def2-TZVP) a dissociation energy of 2 eV for $[Ru(bpy)_3]^{+}$,[55] while our M06-level calculation gives 2.57 eV for $[Ru(bpy)_3]^{+}$ and 4.53 eV for $[Ru(bpy)_3]^{2+}$.

**3.3. Analysis of the IR Spectrum of $[Ru(bpy)_3]^{2+}$.** The experimental IR bands have been assigned with an approximate vibrational mode description from the DFT calculations for both $[Ru(bpy)_3]^{2+}$ and $[Ru(bpy)_3]^{+}$, as listed in Table 1. In the case of $[Ru(bpy)_3]^{2+}$, the IRMPD experiment yields two main bands centered at 1436 and 757 $cm^{-1}$ that are closely predicted at 1424 and 750 $cm^{-1}$, respectively (left panel of Figure 4d). In general, all four levels of theory presented in Figure 4 accurately identify these two main IR bands, although their relative intensities are reversed as compared with experiment. The higher-frequency band shows dominant CC and CN stretch character combined with C−H in-plane bending. The lower-frequency mode is predominantly due to C−H out of plane bending motion. Theoretical bands with lower intensity are not observed in the experimental spectrum, which we attribute to collisional deactivation of the ions by the helium buffer gas inside QIT during IR activation, which prevents ions from reaching the dissociation threshold.[62,66,70,75] Especially for ions with a relatively high


https://dx.doi.org/10.1021/acs.jpca.0c00888
J. Phys. Chem. A 2020, 124, 2449−2459

**Table 1. Experimental Vibrational Frequencies (in $cm^{-1}$) of the $[Ru(bpy)_3]^+$ and $[Ru(bpy)_3]^{2+}$ Systems Compared with Scaled Harmonic Values Computed at the M06 Level[a]**

| | theory | | |
|---|---|---|---|
| experiment (IRMPD) | M06/6-311+G(d,p) | M06/TZ2P | assignments[b] |
| | | $[Ru(bpy)_3]^{2+}$ | |
| | 1583 | 1602 | CC str (s), CN str (w) |
| 1436 (25) | 1424 | 1451 | CC str (s), CN str (w), CHip bend (s) |
| | 1389 | 1437 | CHip bend (s), CC str (s), CN str (w) |
| 757 (9) | 750 | 763 | CHoop bend (s), bpy ring breath (w) |
| | | $[Ru(bpy)_3]^{+}$ | |
| 1549 (~50) | 1550 | 1538 | CC str (s), CN str (w), CHip bend (s) |
| 1427 (33) | 1422 | 1425 | CC str (w), CN str (w), CHip bend (s) |
| 1360 (47) | 1343 | 1342 | |
| 1264[c] (~50) | 1278 | 1240 | NRuN bend (s), CC str (s), CN str (s) |
| 1213 (~42) | 1226 | 1219 | CHip bend (s), CC str (w) |
| | 1215 | 1213 | CHip bend (s), CC str (w) |
| 1073 (60) | 1093 | 1093 | bpy ring breath (w), CHip bend (w) |
| 870 (100) | 917 | 899 | Ru−N sym str (s), bpy ring breath (s), CHip bend (w) |
| | 846 | 855 | bpy-oop (m), CHoop bend (w) |
| 746 (11) | 743 | 758 | NRuN bend (s), bpy ring breath (s), CHoop (s) |
| 627 (41) | 615 | 635 | Ru−N asym str (s), bpy ring deformation (s) |

[a]Values in parentheses are observed IR bandwidths (FWHM in $cm^{-1}$). Mode descriptions for the IR bands indicate the dominant contributions. [b]str, stretch; ip, in-plane bending mode; oop, out-of-plane bending; bpy ring breath, bipyridine ring breathing; sym, symmetric; asym, asymmetric; s, strong band; m, medium; w, weak. [c]Shoulder.

dissociation threshold, such as $[Ru(bpy)_3]^{2+}$, this effect leads to an apparent IRMPD cutoff, empirically indicated with a dashed line in Figure 4a.

IR spectra of $[Ru(bpy)_3]^{2+}$ recorded in a KBr pellet in the 1000−1800 $cm^{-1}$ range were reported by Sun et al.[26] and by Mukuta et al.[49] The dominant IR bands at 1424, 1447, and 1465 $cm^{-1}$ in the pellet spectra[49] are close to our experimental band at 1436 $cm^{-1}$ (fwhm = 25 $cm^{-1}$). Additional low-intensity IR bands were observed in the pellet spectrum[49] at 1314, 1271, and 1161 $cm^{-1}$. These bands were too weak to be observed in our IRMPD spectrum and the IR range below 1000 $cm^{-1}$ was not reported for the pellet spectrum.

**3.4. Analysis of the IR Spectrum of $[Ru(bpy)_3]^+$.** We now turn to the charge-reduced $[Ru(bpy)_3]^+$ ion, for which an experimental IR spectrum has, to the best of our knowledge, not been reported. As discussed above, this singly charged ion has a much lower threshold to dissociation, so that nearly all IR bands predicted by theory can be correlated with bands observed in the IRMPD spectrum, although several bands are significantly shifted in frequency and some have deviating intensities (see right panel of Figure 4). It is notable that spectra computed using different theoretical methods vary more for the monocation than for the dication, both in position and in intensity. The B3LYP calculated spectra are quite similar with small differences depending on the basis set used, but the overall deviation from the experimental spectrum is substantial. A significant improvement is observed for the M06 functional (Figure 4d), perhaps consistent with suggestions on the suitability of this functional for transition metal complexes.[99,100] For instance, the IRMPD band at 1073 $cm^{-1}$ (fwhm = 60 $cm^{-1}$) can be attributed to the band predicted at 1093 $cm^{-1}$ at the M06/6-311+G(d,p) level, while this band is calculated at 1119 $cm^{-1}$ at the B3LYP/def2-TZVP level (Figure 4a). The experimental band at 1213 $cm^{-1}$ agrees well with the M06 predicted band at 1215 $cm^{-1}$. This experimental band has a shoulder at 1264 $cm^{-1}$, which is also closely predicted at 1278 $cm^{-1}$. Finally, the most intense band in the computed spectrum at 917 $cm^{-1}$ is also relatively close to the strong experimental band at 870 $cm^{-1}$.

A very similar infrared spectrum is obtained at the M06/TZ2P level of theory, shown in orange in Figure 4d, although a few differences are noted. At the M06/TZ2P level, the dominant band predicted at 899 $cm^{-1}$ moves closer toward the experimental value; however, the band at 1240 $cm^{-1}$ moves further away from the experimental position. Structural parameters given in Supporting Information Table S1 are very close to those calculated at the M06/6-311+G(d,p) level.

A careful inspection of the normal mode atom displacements shows that all levels of theory yield similar normal mode characters (Table 1). The most intense and strongly broadened experimental band at 870 $cm^{-1}$, assigned to the band calculated at 917 $cm^{-1}$ (M06), is best characterized as a symmetric bpy ring breathing motion that involves a symmetric Ru−N stretching motion (Figure 5). The large 47

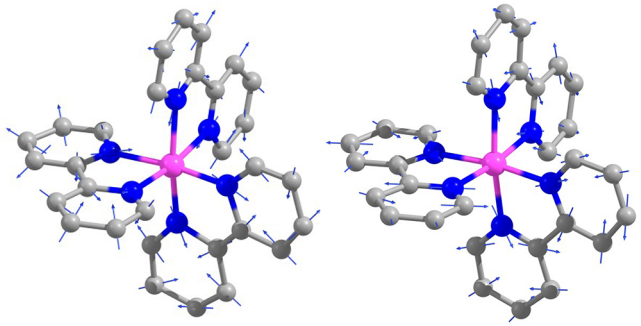


**Figure 5.** Two of the vibrational normal modes for the charge-reduced complex calculated at the M06 level of theory (H atoms omitted for clarity). These modes correspond to the observed IRMPD bands at (a) 870 $cm^{-1}$ (fwhm = 100 $cm^{-1}$) and (b) 1073 $cm^{-1}$ (fwhm = 60 $cm^{-1}$). Theory predicts these bands to be at 917 and 1093 $cm^{-1}$, respectively (see Table 1).

$cm^{-1}$ (29 $cm^{-1}$ at the M06/TZ2P) blue shift with respect to the experiment therefore suggests that the central Ru-ligand coordination bonds are not as strong as theory predicts, which we investigate further here.

The hybrid B3LYP functional uses 20% Hartree−Fock (HF) exact exchange,[101] while M06 has 27% exact exchange.[81,102] Inclusion of higher HF exchange contribution in the DFT functional can lead to overbinding[103] or underbinding[104] of the complexes. Figure 6 illustrates the spectral effects of a gradual reduction of the HF exact-exchange contribution in the B3LYP functional (using the def2-TZVP basis set) starting from the original 20% value. At lower values of HF contribution, the


https://dx.doi.org/10.1021/acs.jpca.0c00888
J. Phys. Chem. A 2020, 124, 2449−2459

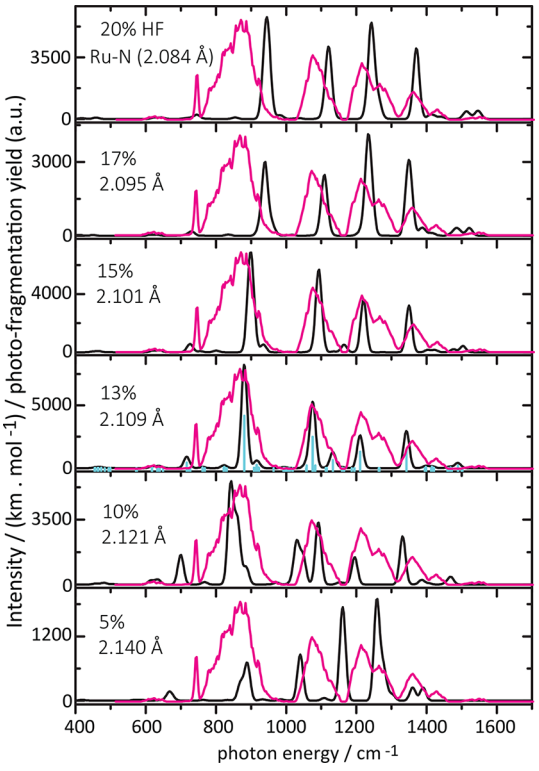


**Figure 6.** Theoretical IR spectra for $[Ru(bpy)_3]^+$ at the B3LYP/def2-TZVP level of theory with varying levels of Hartree−Fock exact-exchange contribution, starting from the 20% default in B3LYP (top panel) down to 5% (bottom panel). The experimental IRMPD spectrum is the magenta trace in each panel. Reducing the HF contribution leads to an increased average Ru − N bond distance, a reduced electrostatic contribution to the metal−ligand binding (not shown), and a gradual red shift of the main bands in the spectrum.

main IR features shift to lower frequencies, in the direction of the experimentally observed positions. Relative intensities also appear to converge toward experimentally observed values. At the same time, the average Ru−N bond length (given in each panel of Figure 6) increases, indicating a weaker metal−ligand bonding at lower HF contribution. Partial charges at the Ru and N atoms also decrease (in an absolute sense) suggesting the reduced binding to be due to reduced electrostatic attraction. The hexadentate coordination is maintained. At an HF contribution of about 13−15%, we qualitatively find an optimum match between experimental and computed IR spectra. The most significant improvements in experimental versus computed frequencies occur for the dominant IR bands. For the 13% HF calculation, the (broadened) bands centered at 870, 1073, and 1213 $cm^{-1}$ are predicted at 880, 1076, and 1210 $cm^{-1}$ with the approximate mode descriptions unchanged from those in Table 1. In addition, the weak and broad experimental feature centered around 625 $cm^{-1}$ is more closely predicted to be due to two absorptions at 618 and 640 $cm^{-1}$. Conversely, the position of the sharp band observed at 746 $cm^{-1}$ appears to be better predicted by the computations including a higher percentage of exact exchange. We conclude that B3LYP/def2TZVP with the reduced HF exact-exchange contribution gives the optimum results in terms of prediction of the IR spectrum. For Fe−ligand complexes, Reiher et al.[104] also suggested to reduce the HF exchange to 15% to better reproduce experimental data, focusing especially on spin multiplicity. Similarly, Moritz et al.[105] reported an improved modeling of the binding of $N_2$ to Sellmann-type Fe(II) compounds upon reducing the default 20% HF to 15%.

**3.5. Structural Parameters of $[Ru(bpy)_3]^{2+}$ and $[Ru(bpy)_3]^+$.** Selected structural parameters resulting from the calculations for both members of the redox pair are summarized in Table 2. For $[Ru(bpy)_3]^{2+}$, the average Ru−N bond length is 2.081 Å and the bpy ligand bite angle with Ru is predicted to be 78.0°. These values can be compared with X-ray data,[106] which indicates that the Ru−N distance is slightly overestimated by 0.016 Å and that the bpy ligand bite angle is correct. The computed gas-phase data are reasonably close to results for an octahedral ligand environment. The ion is thought to have $D_3$ symmetry,[59,107,108] and the geometry optimization without symmetry constraints indeed gives a near-$D_3$ structure (rms deviation = 0.0193; see Figure 2). Upon charge reduction to $[Ru(bpy)_3]^+$, overall structural parameters remain similar, maintaining the pseudo-octahedral geometry of $D_3$ symmetry[55] (rms deviation = 0.0188). The most striking geometry change is perhaps the average Ru−N bond length, which contracts slightly (−0.012 Å) upon charge reduction. Despite the relatively minor structural changes, the IR spectrum changes significantly.

The computed contraction of the Ru−N bond length for $[Ru(bpy)_3]^+$ relative to $[Ru(bpy)_3]^{2+}$ suggests an increased metal−ligand bond energy, which indicates that the additional negative charge resides on the ligands providing an additional attractive Coulomb contribution to the metal−ligand binding. However, IR induced dissociation of $[Ru(bpy)_3]^+$ is much more facile than dissociation of $[Ru(bpy)_3]^{2+}$, clearly suggesting a lower bond dissociation energy. Both observations need not be in contradiction, as the dissociation process leads

**Table 2. Average Ru−N Distances (Å) and N−Ru—N Bond Angles (deg) for $[Ru(bpy)_3]^{2+}$ and $[Ru(bpy)_3]^+$ Compared with Crystallographic Literature Data[106,a]**

| | $[Ru(bpy)_3]^{2+}$ | | | $[Ru(bpy)_3]^+$ | | | |
|---|---|---|---|---|---|---|---|
| parameter | M06/6-311+G(d,p) | B3LYP | exp[106] X-ray crystallography | M06/6- 311+G(d,p) | M06/TZ2P | B3LYP | B3LYP (13% HF) |
| | | | Bond Distance (Å) | | | | |
| $d$(Ru−N) | 2.081(0) | 2.096(0) | 2.065(2) | 2.069(0) | 2.069(0) | 2.084(0) | 2.109(0) |
| | | | Bond Angle (deg) | | | | |
| ∠N−Ru−N′ | 78.0(0) | 77.9(0) | 78.7(1) | 78.4(0) | 78.4(0) | 77.9(0) | 78.3(0) |
| ∠N−Ru−N″ | 88.2(0) | 88.5(1) | 89.1(1) | 89.8(0) | 90.2(2) | 88.5(1) | 89.8(1) |
| ∠N−Ru−N‴ | 173.3(1) | 173.0(0) | 173.0(1) | 172.3(2) | 172.1(2) | 173.0(0) | 172.3(1) |
| ∠N′−Ru−N″ | 97.1(1) | 96.8(4) | 96.3(1) | 96.2(1) | 96.0(1) | 97.0(0) | 96.2(0) |

[a]Values calculated using B3LYP/def2-TZVP with reduced Hartree−Fock exact exchange (13% HF; see text) are also listed for the charge-reduced $[Ru(bpy)_3]^+$ ion. Atom labels are shown in Figure 2. Parenthesized values are standard deviations in units of the last quoted digit.


https://dx.doi.org/10.1021/acs.jpca.0c00888
J. Phys. Chem. A 2020, 124, 2449−2459

to the expulsion of a neutral ligand; the IRMPD product ion corresponds to $[Ru(bpy)_2]^+$.

**3.6. Electronic Structure of $[Ru(bpy)_3]^+$.** A peculiar finding is that the band intensities computed by the M06 functional are about 50 times higher for $[Ru(bpy)_3]^+$ than for $[Ru(bpy)_3]^{2+}$; see Figure 4. At the B3LYP level, a 20−35-fold increase is seen. An unrestricted Hartree−Fock (UHF) calculation gives calculated intensities that are "only" 7 times higher for $[Ru(bpy)_3]^+$ than for $[Ru(bpy)_3]^{2+}$, although the UHF predicted frequencies for $[Ru(bpy)_3]^+$ do not match experimental results (see Supporting Information Figure S1). Such deviations in relative intensities between UHF and DFT levels may be an indication of the DFT results being susceptible to electron self-interaction error (SIE)[109,110] for the open-shell $[Ru(bpy)_3]^+$ ion. This relates to the question of the (de)localization of the added electron upon charge reduction, as for instance investigated for the attachment of an electron to a multiply charged peptide cation by Gilson et al.[110] Conventional DFT functionals (such as the hybrid B3LYP) predict the added unpaired electron to be delocalized over the entire peptide, even upon its imminent dissociation into two fragments, which appears unphysical. However, several *ab initio* methods (UHF, MP2, CCSD) and long-range corrected DFT functionals (e.g., LC-BLYP, CAM-B3LYP[111]) predict the unpaired electron to be localized on the group with highest electron affinity.

We therefore inspect the frontier molecular orbitals of the $[Ru(bpy)_3]^+$ ion in Figure 7, with $[Ru(bpy)_3]^{2+}$ displayed as a reference. The B3LYP/6-311+g(d,p) calculations for the closed-shell 2+ system show that the highest occupied molecular orbital (HOMO) is primarily centered on the Ru atom, while the lowest unoccupied molecular orbital (LUMO) is mostly delocalized over the three bpy ligands. Turning to $[Ru(bpy)_3]^+$, the added electron appears indeed to be injected into the LUMO of the 2+ system, now becoming the singly occupied MO (SOMO) of the radical cation $[Ru(bpy)_3]^+$. B3LYP and M06 functionals (Figure 7b−d) give nearly identical results in which the SOMO is entirely delocalized over the three bpy ligands, as also reported in ref 55. However, using one of the long-range corrected DFT functionals LC-BLYP or CAM-B3LYP, the SOMO is seen to be strongly localized on a single bpy moiety (Figure 7e,f). These observations are also supported by the partial charges resulting from an NPA analysis at the different levels of theory as summarized in Table 3. In addition, the SOMO−1 of $[Ru(bpy)_3]^+$ is mainly localized on the metal center and is very similar to the HOMO of $[Ru(bpy)_3]^{2+}$, except at LC-BLYP and CAM-B3LYP levels, where the amplitude contributions from the ligand orbitals are again more localized.

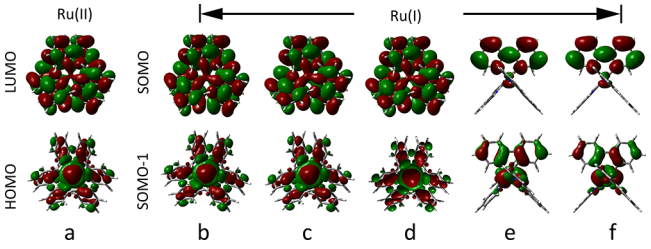


**Figure 7.** B3LYP/6-311+g(d,p) computed HOMO and LUMO of $[Ru(bpy)_3]^{2+}$ (a) and SOMO and SOMO−1 orbitals for the $[Ru(bpy)_3]^+$ ion (b). For the charge-reduced ion, the same MOs calculated at the M06 (c), B3LYP (HF = 13%)/def2-TZVP (d), LC-BLYP/def2-TZVP (e), and CAM-B3LYP/6-311+G(d,p) (f) levels of theory are also shown. Note the more localized character of the orbitals (and hence of the charge; see Table 3) using the latter two functionals. An isosurface value of 0.015 was used for all orbitals.

The more localized character of the SOMO, and hence of the charge, as predicted by the long-range corrected functionals also leads to a geometry that is less symmetrical for the $[Ru(bpy)_3]^+$ complex ion. For instance at the LC-BLYP/def2-TZVP level, the Ru−N bonds of the bpy ligand carrying the localized SOMO are shorter (2.063 Å) than those with the other two bpy ligands (2.082 Å), in agreement with a higher Coulomb attraction to the metal center for the negatively charged bpy unit.

We can now speculate on the origin of the peculiar spectral broadening observed for the main bands in the IRMPD spectrum of $[Ru(bpy)_3]^+$. If we assume that the negative charge localized on one of the ligands can easily hop from one bpy ligand to another, the system may possess a fluxional character, where the three bpy units take turns at attaching the added electron and hence at binding more strongly to the Ru center. At finite temperatures, such a system may show spectrally broadened resonances as IR excitation may enhance the charge hopping and hence the fluxional character of the system. A prototypical example is the vibrational spectrum of the $CH_5^+$ ion, which may be regarded as a complex of a methyl cation and an $H_2$ molecule where the five H atoms are fluxional, which is strongly temperature dependent, in terms of both band positions and widths.[112]

Although the more localized electronic character predicted by LC-BLYP and CAM-B3LYP may thus qualitatively

**Table 3. NPA Partial Charges for Selected Atoms in the 2+ and 1+ Complexes[a]**

| | | B3LYP/6-311+G(d,p) | | M06/6-311+G(d,p) | LC-BLYP/def2-TZVP | CAM-B3LYP/6-311+G(d,p) |
|---|---|---|---|---|---|---|
| | atom | 2+ | 1+ | 1+ | 1+ | 1+ |
| ligand | Ru | 0.160 | 0.161 | 0.144 | 0.069 | 0.139 |
| bpy (1st) | N | −0.379 | −0.389 | −0.400 | −0.401 | −0.453 |
| | N | −0.379 | −0.389 | −0.399 | −0.401 | −0.453 |
| bpy (2nd) | N | −0.379 | −0.388 | −0.400 | −0.310 | −0.371 |
| | N | −0.379 | −0.389 | −0.399 | −0.303 | −0.361 |
| bpy (3rd) | N | −0.379 | −0.388 | −0.400 | −0.310 | −0.371 |
| | N | −0.379 | −0.388 | −0.399 | −0.303 | −0.361 |

[a]Note the similar charges on the Ru atom in the overall 1+ and 2+ complexes, indicating that the added electron is on the ligands. Note also the asymmetric charge distribution over the three ligands with the long-range corrected functionals as compared to the symmetric distribution using B3LYP and M06.


https://dx.doi.org/10.1021/acs.jpca.0c00888
J. Phys. Chem. A 2020, 124, 2449−2459

rationalize the observed bandwidths in the IRMPD spectrum, the predicted frequencies at these levels of theory do not match with the experiment (see Figure S1). We do not further investigate this here but just note that B3LYP and M06 are in general known for their ability to predict vibrational spectra more accurately than many other DFT functionals.

## 4. CONCLUSIONS

We report the first gas-phase IR spectra of isolated $[Ru(bpy)_3]^{2+}$ and its charge-reduced analogue $[Ru(bpy)_3]^{+}$. The energy required to remove a bpy unit from $[Ru(bpy)_3]^{+}$ is clearly much lower than from its oxidized counterpart $[Ru(bpy)_3]^{2+}$. Their IR spectra are also very distinct and while DFT computations have no difficulties reproducing the IR spectrum of the closed-shell dication, the IR spectrum of the monocation contains a large number of bands that appear broadened and that are difficult to reproduce at the DFT levels employed in this study. Reducing the HF exact-exchange contribution in the B3LYP/def2-TZVP calculations, results in a reduced the metal−ligand binding and gives an improved prediction of the experimental IRMPD spectrum. Upon charge reduction, all ligands remain intact and in the same octahedral configuration. Computations using the M06 and B3LYP functionals suggest that the added electron in $[Ru(bpy)_3]^{+}$ is delocalized over all three bpy ligands, while computations using long-range corrected functionals (LC-BLYP and CAM-B3LYP) suggest it to be localized on a single bpy ligand. A more localized charge could lead to a fluxional system that might explain the spectral broadening observed; however, these functionals fail to reproduce the experimentally observed IR spectrum. Hence, we conclude that the IR spectra presented here of the isolated $[Ru(bpy)_3]^{2+/1+}$ redox pair are useful benchmarks for further theoretical investigations on this system. The experimental method of combining electron-transfer reduction and IR ion spectroscopy in an ion trap mass spectrometer is shown to be of interest to investigate isolated metal−ligand complexes in oxidation states that are not readily accessible using standard ESI ion generation.

## ■ ASSOCIATED CONTENT

### Supporting Information

The Supporting Information is available free of charge at https://pubs.acs.org/doi/10.1021/acs.jpca.0c00888.

Table S1, calculated average Ru−N distances and Ru centered bond angles of $[Ru(bpy)_3]^{2+}$ and $[Ru(bpy)_3]^{+}$ ions in the gas phase compared with crystallographic literature data; Figure S1, theoretical IR spectra for $[Ru(bpy)_3]^{+}$ at additional levels of theory compared with the experimental IRMPD spectrum (magenta trace) for the charge-reduced complex ion (PDF)

## ■ AUTHOR INFORMATION


### Corresponding Author

**Jos Oomens** − *Institute for Molecules and Materials, FELIX Laboratory, Radboud University, 6525 ED Nijmegen, The Netherlands; University of Amsterdam, 1098XH Amsterdam, The Netherlands;* orcid.org/0000-0002-2717-1278; Email: j.oomens@science.ru.nl

### Authors

**Musleh Uddin Munshi** − *Institute for Molecules and Materials, FELIX Laboratory, Radboud University, 6525 ED Nijmegen, The Netherlands;* orcid.org/0000-0001-9197-8490

**Jonathan Martens** − *Institute for Molecules and Materials, FELIX Laboratory, Radboud University, 6525 ED Nijmegen, The Netherlands;* orcid.org/0000-0001-9537-4117

**Giel Berden** − *Institute for Molecules and Materials, FELIX Laboratory, Radboud University, 6525 ED Nijmegen, The Netherlands;* orcid.org/0000-0003-1500-922X

Complete contact information is available at: https://pubs.acs.org/10.1021/acs.jpca.0c00888


### Notes

The authors declare no competing financial interest.

## ■ ACKNOWLEDGMENTS

We gratefully acknowledge the *Nederlandse Organisatie voor Wetenschappelijk Onderzoek (NWO)* for the support of the FELIX Laboratory and the FELIX staff for their assistance. Financial support for this project was provided by NWO Chemical Sciences under VICI project no. 724.011.002. We also thank NWO Physical Sciences (EW) and the SurfSARA Supercomputer Centre for providing the computational time and resources (grant no. 2019.062). We thank Profs. G. C. Groenenboom (Radboud University, Nijmegen) and L. Visscher (Free University, Amsterdam) for the many helpful discussions.

## ■ REFERENCES


(1) Grätzel, M. Photoelectrochemical Cells. *Nature* **2001**, *414*, 338−344.

(2) Grätzel, M. Dye-Sensitized Solar Cells. *J. Photochem. Photobiol., C* **2003**, *4*, 145−153.

(3) Grätzel, M. Solar Energy Conversion by Dye-Sensitized Photovoltaic Cells. *Inorg. Chem.* **2005**, *44*, 6841−6851.

(4) Hagfeldt, A.; Boschloo, G.; Sun, L.; Kloo, L.; Pettersson, H. Dye-Sensitized Solar Cells. *Chem. Rev.* **2010**, *110*, 6595−6663.

(5) Kalyanasundaram, K. Photophysics, Photochemistry and Solar Energy Conversion with Tris(Bipyridyl) Ruthenium(II) and Its Analogues. *Coord. Chem. Rev.* **1982**, *46*, 159−244.

(6) Kalyanasundaram, K.; Grätzel, M. Applications of Functionalized Transition Metal Complexes in Photonic and Optoelectronic Devices. *Coord. Chem. Rev.* **1998**, *177*, 347−414.

(7) Beer, P. D.; Cadman, J. Electrochemical and Optical Sensing of Anions by Transition Metal Based Receptors. *Coord. Chem. Rev.* **2000**, *205*, 131−155.

(8) Vos, J. G.; Kelly, J. M. Ruthenium Polypyridyl Chemistry; from Basic Research to Applications and Back Again. *Dalton Trans.* **2006**, *0*, 4869−4883.

(9) Prier, C. K.; Rankic, D. A.; MacMillan, D. W. Visible Light Photoredox Catalysis with Transition Metal Complexes: Applications in Organic Synthesis. *Chem. Rev.* **2013**, *113*, 5322−5363.

(10) Schultz, D. M.; Yoon, T. P. Solar Synthesis: Prospects in Visible Light Photocatalysis. *Science* **2014**, *343*, 1239176.

(11) Twilton, J.; Zhang, P.; Shaw, M. H.; Evans, R. W.; MacMillan, D. W. The Merger of Transition Metal and Photocatalysis. *Nat. Rev. Chem.* **2017**, *1*, 0052.

(12) Concepcion, J. J.; Jurss, J. W.; Brennaman, M. K.; Hoertz, P. G.; Patrocinio, A. O. T.; Murakami Iha, N. Y.; Templeton, J. L.; Meyer, T. J. Making Oxygen with Ruthenium Complexes. *Acc. Chem. Res.* **2009**, *42*, 1954−1965.

(13) Wasylenko, D. J.; Ganesamoorthy, C.; Koivisto, B. D.; Henderson, M. A.; Berlinguette, C. P. Insight into Water Oxidation by Mononuclear Polypyridyl Ru Catalysts. *Inorg. Chem.* **2010**, *49*, 2202−2209.

(14) Alstrum-Acevedo, J. H.; Brennaman, M. K.; Meyer, T. J. Chemical Approaches to Artificial Photosynthesis. *Inorg. Chem.* **2005**, *44*, 6802−6827.
(15) Balzani, V.; Juris, A.; Venturi, M.; Campagna, S.; Serroni, S. Luminescent and Redox-Active Polynuclear Transition Metal Complexes. *Chem. Rev.* **1996**, *96*, 759−834.
(16) Boschloo, G.; Hagfeldt, A. Characteristics of the Iodide/Triiodide Redox Mediator in Dye-Sensitized Solar Cells. *Acc. Chem. Res.* **2009**, *42*, 1819−1826.
(17) Pashaei, B.; Shahroosvand, H.; Abbasi, P. Transition Metal Complex Redox Shuttles for Dyesensitized Solar Cells. *RSC Adv.* **2015**, *5*, 94814−94848.
(18) Ceroni, P.; Bergamini, G.; Balzani, V. Old Molecules, New Concepts:$[Ru(bpy)_3]^{2+}$ as a Molecular Encoder−Decoder. *Angew. Chem.* **2009**, *121*, 8668−8670.
(19) Juris, A.; Balzani, V.; Barigelletti, F.; Campagna, S.; Belser, P. l.; von Zelewsky, A. Ru(II) Polypyridine Complexes: Photophysics, Photochemistry, Eletrochemistry, and Chemiluminescence. *Coord. Chem. Rev.* **1988**, *84*, 85−277.
(20) Angell, S. E.; Zhang, Y.; Rogers, C. W.; Wolf, M. O.; Jones, W. E. Photophysical Properties of Ru(II) Bipyridyl Complexes Containing Hemilabile Phosphine− Ether Ligands. *Inorg. Chem.* **2005**, *44*, 7377−7384.
(21) Medlycott, E. A.; Hanan, G. S. Designing Tridentate Ligands for Ruthenium(II) Complexes with Prolonged Room Temperature Luminescence Lifetimes. *Chem. Soc. Rev.* **2005**, *34*, 133−142.
(22) Kuciauskas, D.; Monat, J. E.; Villahermosa, R.; Gray, H. B.; Lewis, N. S.; McCusker, J. K. Transient Absorption Spectroscopy of Ruthenium and Osmium Polypyridyl Complexes Adsorbed onto Nanocrystalline $TiO_2$ Photoelectrodes. *J. Phys. Chem. B* **2002**, *106*, 9347−9358.
(23) Del Guerzo; Leroy, S.; Fages, F.; Schmehl, R. H. Photophysics of Re(I) and Ru(II) Diimine Complexes Covalently Linked to Pyrene: Contributions from Intra-Ligand Charge Transfer States. *Inorg. Chem.* **2002**, *41*, 359−366.
(24) Wang, X.-Y.; Del Guerzo, A.; Tunuguntla, H.; Schmehl, R. H. Photophysical Behavior of Ru(II) and Os(II) Terpyridyl Phenylene Vinylene Complexes: Perturbation of MLCT State by Intra-Ligand Charge-Transfer State. *Res. Chem. Intermed.* **2007**, *33*, 63−77.
(25) Yeh, A. T.; Shank, C. V.; McCusker, J. K. Ultrafast Electron Localization Dynamics Following Photo-Induced Charge Transfer. *Science* **2000**, *289*, 935−938.
(26) Sun, Q.; Dereka, B.; Vauthey, E.; Daku, L. M. L.; Hauser, A. Ultrafast Transient IR Spectroscopy and DFT Calculations of Ruthenium (II) Polypyridyl Complexes. *Chem. Sci.* **2017**, *8*, 223−230.
(27) Nazeeruddin, M. K.; Kay, A.; Rodicio, I.; Humphry-Baker, R.; Müller, E.; Liska, P.; Vlachopoulos, N.; Grätzel, M. Conversion of Light to Electricity by Cis-$X_2$bis(2,2′-Bipyridyl-4,4′-Dicarboxylate) Ruthenium(II) Charge-Transfer Sensitizers (X= $Cl^-$, $Br^-$, $I^-$, $CN^-$, and $SCN^-$) on Nanocrystalline Titanium Dioxide Electrodes. *J. Am. Chem. Soc.* **1993**, *115*, 6382−6390.
(28) Nazeeruddin, M. K.; Pechy, P.; Renouard, T.; Zakeeruddin, S. M.; Humphry-Baker, R.; Comte, P.; Liska, P.; Cevey, L.; Costa, E.; Shklover, V. Engineering of Efficient Panchromatic Sensitizers for Nanocrystalline $TiO_2$-Based Solar Cells. *J. Am. Chem. Soc.* **2001**, *123*, 1613−1624.
(29) Tributsch, H. Dye Sensitization Solar Cells: A Critical Assessment of the Learning Curve. *Coord. Chem. Rev.* **2004**, *248*, 1511−1530.
(30) Grünwald, R.; Tributsch, H. Mechanisms of Instability in Ru-Based Dye Sensitization Solar Cells. *J. Phys. Chem. B* **1997**, *101*, 2564−2575.
(31) Harikisun, R.; Desilvestro, H. Long-Term Stability of Dye Solar Cells. *Sol. Energy* **2011**, *85*, 1179−1188.
(32) Bomben, P. G.; Robson, K. C.; Sedach, P. A.; Berlinguette, C. P. On the Viability of Cyclometalated Ru(II) Complexes for Light-Harvesting Applications. *Inorg. Chem.* **2009**, *48*, 9631−9643.
(33) Koivisto, B. D.; Robson, K. C.; Berlinguette, C. P. Systematic Manipulation of the Light-Harvesting Properties for Tridentate Cyclometalated Ruthenium(II) Complexes. *Inorg. Chem.* **2009**, *48*, 9644−9652.
(34) Bessho, T.; Yoneda, E.; Yum, J.-H.; Guglielmi, M.; Tavernelli, I.; Imai, H.; Rothlisberger, U.; Nazeeruddin, M. K.; Grätzel, M. New Paradigm in Molecular Engineering of Sensitizers for Solar Cell Applications. *J. Am. Chem. Soc.* **2009**, *131*, 5930−5934.
(35) Bomben, P. G.; Koivisto, B. D.; Berlinguette, C. P. Cyclometalated Ru Complexes of Type $[Ru^{II}(N\wedge N)_2(C\wedge N)]^Z$: Physicochemical Response to Substituents Installed on the Anionic Ligand. *Inorg. Chem.* **2010**, *49*, 4960−4971.
(36) Bomben, P. G.; Thériault, K. D.; Berlinguette, C. P. Strategies for Optimizing the Performance of Cyclometalated Ruthenium Sensitizers for Dye-Sensitized Solar Cells. *Eur. J. Inorg. Chem.* **2011**, *2011*, 1806−1814.
(37) Robson, K. C.; Koivisto, B. D.; Yella, A.; Sporinova, B.; Nazeeruddin, M. K.; Baumgartner, T.; Grätzel, M.; Berlinguette, C. P. Design and Development of Functionalized Cyclometalated Ruthenium Chromophores for Light-Harvesting Applications. *Inorg. Chem.* **2011**, *50*, 5494−5508.
(38) Robson, K. C.; Sporinova, B.; Koivisto, B. D.; Schott, E.; Brown, D. G.; Berlinguette, C. P. Systematic Modulation of a Bichromic Cyclometalated Ruthenium(II) Scaffold Bearing a Redox-Active Triphenylamine Constituent. *Inorg. Chem.* **2011**, *50*, 6019−6028.
(39) Wadman, S. H.; Kroon, J. M.; Bakker, K.; Lutz, M.; Spek, A. L.; van Klink, G. P.; van Koten, G. Cyclometalated Ruthenium Complexes for Sensitizing Nanocrystalline $TiO_2$ Solar Cells. *Chem. Commun.* **2007**, *2007*, 1907−1909.
(40) Bomben, P. G.; Gordon, T. J.; Schott, E.; Berlinguette, C. P. A Trisheteroleptic Cyclometalated $Ru^{II}$ Sensitizer That Enables High Power Output in a Dye-Sensitized Solar Cell. *Angew. Chem.* **2011**, *123*, 10870−10873.
(41) Wadman, S. H.; Lutz, M.; Tooke, D. M.; Spek, A. L.; Hartl, F. E.; Havenith, R. W.; van Klink, G. P.; van Koten, G. Consequences of N, C, N′-and C, N, N′-Coordination Modes on Electronic and Photophysical Properties of Cyclometalated Aryl Ruthenium(II) Complexes. *Inorg. Chem.* **2009**, *48*, 1887−1900.
(42) Sauvage, J. P.; Collin, J. P.; Chambron, J. C.; Guillerez, S.; Coudret, C.; Balzani, V.; Barigelletti, F.; De Cola, L.; Flamigni, L. Ruthenium(II) and Osmium(II) Bis(Terpyridine) Complexes in Covalently-Linked Multicomponent Systems: Synthesis, Electrochemical Behavior, Absorption Spectra, and Photochemical and Photophysical Properties. *Chem. Rev.* **1994**, *94*, 993−1019.
(43) Forster, M.; Hester, R. E. Resonance Raman Investigation of Electronically Excited Ru(Bipyridine)$_3^{2+}$ Using a cw Laser. *Chem. Phys. Lett.* **1981**, *81*, 42−47.
(44) Musgrave, M.; Pople, J. A. A General Valence Force Field for Diamond. *Proc. R. Soc. London A* **1962**, *268*, 474−484.
(45) Grosse, F.; Neugebauer, J. Limits and Accuracy of Valence Force Field Models for $In_xGa_{1-x}N$ Alloys. *Phys. Rev. B: Condens. Matter Mater. Phys.* **2001**, *63*, 085207.
(46) Mallick, P. K.; Danzer, G. D.; Strommen, D. P.; Kincaid, J. R. Vibrational Spectra and Normal-Coordinate Analysis of Tris-(Bipyridine) Ruthenium(II). *J. Phys. Chem.* **1988**, *92*, 5628−5634.
(47) Butler, J. M.; George, M. W.; Schoonover, J. R.; Dattelbaum, D. M.; Meyer, T. J. Application of Transient Infrared and near Infrared Spectroscopy to Transition Metal Complex Excited States and Intermediates. *Coord. Chem. Rev.* **2007**, *251*, 492−514.
(48) Schoonover, J. R.; Bignozzi, C. A.; Meyer, T. J. Application of Transient Vibrational Spectroscopies to the Excited States of Metal Polypyridyl Complexes. *Coord. Chem. Rev.* **1997**, *165*, 239−266.
(49) Mukuta, T.; Fukazawa, N.; Murata, K.; Inagaki, A.; Akita, M.; Tanaka, S. i.; Koshihara, S.-y.; Onda, K. Infrared Vibrational Spectroscopy of $[Ru(bpy)_2(bpm)]^{2+}$ and $[Ru(bpy)_3]^{2+}$ in the Excited Triplet State. *Inorg. Chem.* **2014**, *53*, 2481−2490.
(50) Omberg, K. M.; Schoonover, J. R.; Treadway, J. A.; Leasure, R. M.; Dyer, R. B.; Meyer, T. J. Mid-Infrared Spectrum of $[Ru(bpy)_3]^{2+}$. *J. Am. Chem. Soc.* **1997**, *119*, 7013−7018.


https://dx.doi.org/10.1021/acs.jpca.0c00888
J. Phys. Chem. A 2020, 124, 2449−2459

(51) Cannizzo, A.; van Mourik, F.; Gawelda, W.; Zgrablic, G.; Bressler, C.; Chergui, M. Broadband Femtosecond Fluorescence Spectroscopy of $[Ru(bpy)_3]^{2+}$. *Angew. Chem.* **2006**, *118*, 3246−3248.
(52) Motten, A. G.; Hanck, K.; DeArmound, M. K. ESR of the Reduction Products of $[Fe(bpy)_3]^{2+}$ and $[Ru(bpy)_3]^{2+}$. *Chem. Phys. Lett.* **1981**, *79*, 541−546.
(53) Heath, G. A.; Yellowlees, L. J.; Braterman, P. S. Spectro-Electrochemical Studies on Tris-Bipyridyl Ruthenium Complexes; Ultra-Violet, Visible and near-Infrared Spectra of the Series $[Ru(Bipyridyl)_3]^{2+/1+/0/1-}$. *J. Chem. Soc., Chem. Commun.* **1981**, 287−289.
(54) Noble, B.; Peacock, R. D. Absorption, Circular Dichroism, and Luminescence Spectroscopy of Electrogenerated Δ-$[Ru(bipy)_3]^{+/0/-}$ and Δ-$[Os(bipy)_3]^{+/0/-}$ (bipy = 2,2′-Bipyridine). *Inorg. Chem.* **1996**, *35*, 1616−1620.
(55) Byskov, C. S.; Weber, J. M.; Nielsen, S. B. Gas-Phase Spectroscopy of Singly Reduced Tris(Bipyridine) Ruthenium Ions, $Ru(bipy)_3^+$. *Phys. Chem. Chem. Phys.* **2015**, *17*, 5561−5564.
(56) Stockett, M.; Nielsen, S. Does a Single $CH_3CN$ Molecule Attached to $Ru(bipy)_3^{2+}$ Affect Its Absorption Spectrum? *J. Chem. Phys.* **2015**, *142*, 171102.
(57) Mayoh, B.; Day, P. The Excited States of Bipyridyl and Phenanthroline Complexes of Fe(III), Ru(II) and Ru(III): A Molecular Orbital Study. *Theor. Chem. Acc.* **1978**, *49*, 259−275.
(58) Barigelletti, F.; Juris, A.; Balzani, V.; Belser, P.; Von Zelewsky, A. Excited-State Properties of Complexes of the Tris (Diimine) Ruthenium(2+) Ion Family. *Inorg. Chem.* **1983**, *22*, 3335−3339.
(59) Ferguson, J.; Herren, F. A Model for the Interpretation of the Electronic Spectra of the Complex Ions $M(bpy)_3^{2+}$(M= Fe, Ru, Os) in $D_3$ and $C_2$ Sites. *Chem. Phys.* **1983**, *76*, 45−59.
(60) Rillema, D. P.; Allen, G.; Meyer, T.; Conrad, D. Redox Properties of Ruthenium(II) Tris Chelate Complexes Containing the Ligands 2,2′-Bipyrazine, 2,2′-Bipyridine, and 2,2′-Bipyrimidine. *Inorg. Chem.* **1983**, *22*, 1617−1622.
(61) Garand, E. Spectroscopy of Reactive Complexes and Solvated Clusters: A Bottom-up Approach Using Cryogenic Ion Traps. *J. Phys. Chem. A* **2018**, *122*, 6479−6490.
(62) Martens, J.; Berden, G.; Gebhardt, C. R.; Oomens, J. Infrared Ion Spectroscopy in a Modified Quadrupole Ion Trap Mass Spectrometer at the FELIX Free Electron Laser Laboratory. *Rev. Sci. Instrum.* **2016**, *87*, 103108.
(63) Oomens, J.; Sartakov, B. G.; Meijer, G.; Von Helden, G. Gas-Phase Infrared Multiple Photon Dissociation Spectroscopy of Mass-Selected Molecular Ions. *Int. J. Mass Spectrom.* **2006**, *254*, 1−19.
(64) Martens, J.; Grzetic, J.; Berden, G.; Oomens, J. Structural Identification of Electron Transfer Dissociation Products in Mass Spectrometry Using Infrared Ion Spectroscopy. *Nat. Commun.* **2016**, *7*, 11754.
(65) Foreman, D. J.; McLuckey, S. A. Recent Developments in Gas-Phase Ion/Ion Reactions for Analytical Mass Spectrometry. *Anal. Chem.* **2020**, *92*, 252−266.
(66) Munshi, M. U.; Craig, S. M.; Berden, G.; Martens, J.; DeBlase, A. F.; Foreman, D. J.; McLuckey, S. A.; Oomens, J.; Johnson, M. A. Preparation of Labile $Ni^+$(Cyclam) Cations in the Gas Phase Using Electron Transfer Reduction through Ion-Ion Recombination in an Ion Trap and Structural Characterization with Vibrational Spectroscopy. *J. Phys. Chem. Lett.* **2017**, *8*, 5047−5052.
(67) Kirketerp, M.-B. S.; Nielsen, S. B. Absorption Spectrum of Isolated Tris (2,2′-Bipyridine) Ruthenium(II) Dications in Vacuo. *Int. J. Mass Spectrom.* **2010**, *297*, 63−66.
(68) Xu, S.; Smith, J. E.; Weber, J. M. Uv Spectra of Tris (2,2′-Bipyridine)−M(II) Complex Ions in Vacuo (M= Mn, Fe, Co, Ni, Cu, Zn). *Inorg. Chem.* **2016**, *55*, 11937−11943.
(69) Xu, S.; Weber, J. M. Absorption Spectrum of a Ru(II)-Aquo Complex in Vacuo: Resolving Individual Charge-Transfer Transitions. *J. Phys. Chem. A* **2015**, *119*, 11509−11513.
(70) Munshi, M. U.; Berden, G.; Martens, J. K.; Oomens, J. Gas-Phase Vibrational Spectroscopy of Triphenylamine: The Effect of Charge on Structure and Spectra. *Phys. Chem. Chem. Phys.* **2017**, *19*, 19881−19889.
(71) Martens, J.; Berden, G.; Oomens, J. Structures of Fluoranthene Reagent Anions Used in Electron Transfer Dissociation and Proton Transfer Reaction Tandem Mass Spectrometry. *Anal. Chem.* **2016**, *88*, 6126−6129.
(72) Oepts, D.; Van der Meer, A. F. G.; Van Amersfoort, P. The Free-Electron-Laser User Facility FELIX. *Infrared Phys. Technol.* **1995**, *36*, 297−308.
(73) Knippels, G. M.H.; Van Der Meer, A. F. G. FEL Diagnostics and User Control. *Nucl. Instrum. Methods Phys. Res., Sect. B* **1998**, *144*, 32−39.
(74) Lucas, B.; Gregoire, G.; Lemaire, J.; Maitre, P.; Glotin, F.; Schermann, J.; Desfrancois, C. Infrared Multiphoton Dissociation Spectroscopy of Protonated N-Acetyl-Alanine and Alanyl-Histidine. *Int. J. Mass Spectrom.* **2005**, *243*, 105−113.
(75) Berden, G.; Derksen, M.; Houthuijs, K. J.; Martens, J.; Oomens, J. An Automatic Variable Laser Attenuator for IRMPD Spectroscopy and Analysis of Power-Dependence in Fragmentation Spectra. *Int. J. Mass Spectrom.* **2019**, *443*, 1−8.
(76) Lee, C.; Yang, W.; Parr, R. G. Development of the Colle-Salvetti Correlation-Energy Formula into a Functional of the Electron Density. *Phys. Rev. B: Condens. Matter Mater. Phys.* **1988**, *37*, 785.
(77) Becke, A. D. Becke's Three Parameter Hybrid Method Using the LYP Correlation Functional. *J. Chem. Phys.* **1993**, *98*, 5648−5652.
(78) Cohen, A. J.; Mori-Sánchez, P.; Yang, W. Challenges for Density Functional Theory. *Chem. Rev.* **2012**, *112*, 289−320.
(79) Weigend, F.; Ahlrichs, R. Balanced Basis Sets of Split Valence, Triple Zeta Valence and Quadruple Zeta Valence Quality for H to Rn: Design and Assessment of Accuracy. *Phys. Chem. Chem. Phys.* **2005**, *7*, 3297−3305.
(80) Iikura, H.; Tsuneda, T.; Yanai, T.; Hirao, K. A Long-Range Correction Scheme for Generalized-Gradient-Approximation Exchange Functionals. *J. Chem. Phys.* **2001**, *115*, 3540−3544.
(81) Peverati, R.; Truhlar, D. G. Quest for a Universal Density Functional: The Accuracy of Density Functionals across a Broad Spectrum of Databases in Chemistry and Physics. *Philos. Trans. R. Soc., A* **2014**, *372*, 20120476.
(82) Rassolov, V. A.; Ratner, M. A.; Pople, J. A.; Redfern, P. C.; Curtiss, L. A. 6-31G* Basis Set for Third-Row Atoms. *J. Comput. Chem.* **2001**, *22*, 976−984.
(83) Peterson, K. A. Systematically Convergent Basis Sets with Relativistic Pseudopotentials. I. Correlation Consistent Basis Sets for the Post-*d* Group 13−15 Elements. *J. Chem. Phys.* **2003**, *119*, 11099−11112.
(84) Reed, A. E.; Weinstock, R. B.; Weinhold, F. Natural Population Analysis. *J. Chem. Phys.* **1985**, *83*, 735−746.
(85) Frisch, M. J.; Trucks, G. W.; Schlegel, H. B.; Scuseria, G. E.; Robb, M. A.; Cheeseman, J. R.; Scalmani, G.; Barone, V.; Mennucci, B.; Petersson, G. A., et al. *Gaussian 09*, Revision D.01; Gaussian, Inc.: Wallingford, CT, 2013.
(86) Te Velde, G.; Baerends, E. J. Numerical Integration for Polyatomic Systems. *J. Comput. Phys.* **1992**, *99*, 84−98.
(87) Cossi, M.; Rega, N.; Scalmani, G.; Barone, V. Energies, Structures, and Electronic Properties of Molecules in Solution with the C-PCM Solvation Model. *J. Comput. Chem.* **2003**, *24*, 669−681.
(88) Baerends, E.; Ellis, D.; Ros, P. Self-Consistent Molecular Hartree—Fock—Slater Calculations I. The Computational Procedure. *Chem. Phys.* **1973**, *2*, 41−51.
(89) Cohen, A. J.; Handy, N. C. Dynamic Correlation. *Mol. Phys.* **2001**, *99*, 607−615.
(90) Van Lenthe, E.; Baerends, E. J. Optimized Slater-Type Basis Sets for the Elements 1−118. *J. Comput. Chem.* **2003**, *24*, 1142−1156.
(91) Lenthe, E. v.; Baerends, E. J.; Snijders, J. G. Relativistic Regular Two-Component Hamiltonians. *J. Chem. Phys.* **1993**, *99*, 4597−4610.
(92) van Lenthe, E.; Ehlers, A.; Baerends, E.-J. Geometry Optimizations in the Zero Order Regular Approximation for Relativistic Effects. *J. Chem. Phys.* **1999**, *110*, 8943−8953.


https://dx.doi.org/10.1021/acs.jpca.0c00888
J. Phys. Chem. A 2020, 124, 2449−2459

(93) van Lenthe, E. v.; Snijders, J.; Baerends, E.-J. The Zero-Order Regular Approximation for Relativistic Effects: The Effect of Spin−Orbit Coupling in Closed Shell Molecules. *J. Chem. Phys.* **1996**, *105*, 6505−6516.
(94) van Lenthe, E.; Baerends, E.-J.; Snijders, J. G. Relativistic Total Energy Using Regular Approximations. *J. Chem. Phys.* **1994**, *101*, 9783−9792.
(95) Munshi, M. U.; Martens, J.; Berden, G.; Oomens, J. Gas-Phase Infrared Ion Spectroscopy Characterization of Cu(II/I)Cyclam and Cu(II/I)2,2′-Bipyridine Redox Pairs. *J. Phys. Chem. A* **2019**, *123*, 4149−4157.
(96) Rannulu, N. S.; Rodgers, M. T. Noncovalent Interactions of $Zn^+$ with N-Donor Ligands (Pyridine, 4,4′-Dipyridyl, 2,2′-Dipyridyl, and 1,10-Phenanthroline): Collision-Induced Dissociation and Theoretical Studies. *J. Phys. Chem. A* **2012**, *116*, 1319−1332.
(97) Rannulu, N. S.; Rodgers, M. T. Noncovalent Interactions of $Ni^+$ with N-Donor Ligands (Pyridine, 4,4′-Dipyridyl, 2,2′-Dipyridyl, and 1,10-Phenanthroline): Collision-Induced Dissociation and Theoretical Studies. *J. Phys. Chem. A* **2009**, *113*, 4534−4548.
(98) Rannulu, N. S.; Rodgers, M. T. Noncovalent Interactions of $Cu^+$ with N-Donor Ligands (Pyridine, 4,4-Dipyridyl, 2,2-Dipyridyl, and 1,10-Phenanthroline): Collision-Induced Dissociation and Theoretical Studies. *J. Phys. Chem. A* **2007**, *111*, 3465−3479.
(99) Cramer, C. J.; Truhlar, D. G. Density Functional Theory for Transition Metals and Transition Metal Chemistry. *Phys. Chem. Chem. Phys.* **2009**, *11*, 10757−10816.
(100) Zhao, Y.; Truhlar, D. G. Density Functionals with Broad Applicability in Chemistry. *Acc. Chem. Res.* **2008**, *41*, 157−167.
(101) Becke, A. D. Density-Functional Thermochemistry. III. The Role of Exact Exchange. *J. Chem. Phys.* **1993**, *98*, 5648−5652.
(102) Shao, Y.; Gan, Z.; Epifanovsky, E.; Gilbert, A. T.; Wormit, M.; Kussmann, J.; Lange, A. W.; Behn, A.; Deng, J.; Feng, X. Advances in Molecular Quantum Chemistry Contained in the Q-Chem 4 Program Package. *Mol. Phys.* **2015**, *113*, 184−215.
(103) Csonka, G. I.; Perdew, J. P.; Ruzsinszky, A. Global Hybrid Functionals: A Look at the Engine under the Hood. *J. Chem. Theory Comput.* **2010**, *6*, 3688−3703.
(104) Reiher, M.; Salomon, O.; Hess, B. A. Reparameterization of Hybrid Functionals Based on Energy Differences of States of Different Multiplicity. *Theor. Chem. Acc.* **2001**, *107*, 48−55.
(105) Moritz, G.; Reiher, M.; Hess, B. A. Analysis of Spin States, Spin Barriers, and Trans-Effects Involved in the Coordination and Stabilization of Dinitrogen by Biomimetic Iron Complexes. *Theor. Chem. Acc.* **2005**, *114*, 76−83.
(106) Rillema, D. P.; Jones, D. S.; Woods, C.; Levy, H. A. Comparison of the Crystal Structures of Tris Heterocyclic Ligand Complexes of Ruthenium(II). *Inorg. Chem.* **1992**, *31*, 2935−2938.
(107) Daul, C.; Baerends, E.-J.; Vernooijs, P. A Density-Functional Study of the MLCT States of $[Ru(bpy)_3]^{2+}$ in $D_3$ Symmetry. *Inorg. Chem.* **1994**, *33*, 3538−3543.
(108) Xu, S.; Smith, J. E. T.; Gozem, S.; Krylov, A. I.; Weber, J. M. Electronic Spectra of Tris(2,2′-Bipyridine)-M(II) Complex Ions in Vacuo (M = Fe and Os). *Inorg. Chem.* **2017**, *56*, 7029−7037.
(109) Perdew, J. P.; Zunger, A. Self-Interaction Correction to Density-Functional Approximations for Many-Electron Systems. *Phys. Rev. B: Condens. Matter Mater. Phys.* **1981**, *23*, 5048.
(110) Gilson, A. I.; Van Der Rest, G.; Chamot-Rooke, J.; Kurlancheek, W.; Head-Gordon, M.; Jacquemin, D.; Frison, G. Ground Electronic State of Peptide Cation Radicals: A Delocalized Unpaired Electron? *J. Phys. Chem. Lett.* **2011**, *2*, 1426−1431.
(111) Yanai, T.; Tew, D. P.; Handy, N. C. A New Hybrid Exchange−Correlation Functional Using the Coulomb-Attenuating Method (CAM-B3LYP). *Chem. Phys. Lett.* **2004**, *393*, 51−57.
(112) Asvany, O.; Kumar, P.; Redlich, B.; Hegemann, I.; Schlemmer, S.; Marx, D. Understanding the Infrared Spectrum of Bare $CH_5^+$. *Science* **2005**, *309*, 1219−1222.


https://dx.doi.org/10.1021/acs.jpca.0c00888
J. Phys. Chem. A 2020, 124, 2449−2459